We are IntechOpen,
the world's leading publisher of
Open Access books
Built by scientists, for scientists

6,900
Open access books available

186,000
International authors and editors

200M
Downloads

Our authors are among the

154
Countries delivered to

TOP 1%
most cited scientists

12.2%
Contributors from top 500 universities

CLARIVATE ANALYTICS
BOOK CITATION INDEX
INDEXED

WEB OF SCIENCE™

Selection of our books indexed in the Book Citation Index
in Web of Science™ Core Collection (BKCI)

Interested in publishing with us?
Contact book.department@intechopen.com

Numbers displayed above are based on latest data collected.
For more information visit www.intechopen.com

Applications of Artificial Magnetic Conductors in Monopole and Dipole Antennas

Amir Jafargholi[1], Mahmood Rafaei Booket[2] and Mehdi Veysi[1]
[1]K.N. Toosi University of Technology
[2]Tarbiat Modares University
Iran

1. Introduction

In recent years, introducing metamaterials based on theory established by Veselago, opened the way for many researcher groups to enhance the antenna performances (Veselago, 1968; Veysi et al., 2010; Rafaei et al., 2010; Veysi et al., 2011; Rafaei et al., 2011; Jafargholi et al., 2010; Jafargholi et al., 2011). A standard procedure has been also established for the design of bulk artificial media with negative macroscopic permeability and permittivity. In the past few years, extensive research has been carried out on the metamaterial realization of the artificial magnetic conductors (AMCs) (Jafargholi et al., 2010; McVay et al., 2004). As revealed in (Erentok et al., 2005), the artificial magnetic conductor can be also realized using a volumetric metamaterial constructed from a periodic arrangement of the capacitively loaded loop (CLL) elements. Recently, it has found interesting applications in antenna engineering (Ziolkowski et al., 2003). Due to unique electromagnetic properties, metamaterials have been widely considered in monopole and dipole antennas to improve their performance (Ziolkowski et al., 2003; Liu et al., 2009; Rogers et al., 2003).

This chapter is mainly focused on two different applications of artificial magnetic conductors in the field of dipole pattern modification and dual and multiband dipole antennas. At first, the radiation patterns of the monopole and dipole antennas have been considered, especially at the second harmonic of the main resonant frequency. A closer examination on the PMC structures reveals that they can be used to modify the monopole and dipole radiation patterns. To this aim, the CLLs have been used to realize perfect magnetic conductor.

Finally, this chapter examines reactive loading technique to achieve dual band operation and further size reduction for double-sided printed dipole antennas. Here, the reactive loads are realized by two balanced CLLs placed close to the edge of the printed dipole antenna.

2. Pattern modification of monopole antenna

The linearly polarized and omnidirectional radiation pattern of a vertical monopole antenna has led to a wide range of applications in wireless communications such as wireless local area network (WLAN) and radio broadcast. It is known that the long monopole antennas ($\geq\lambda/2$) suffer from the 180 phase reversal. The fields radiated by reverse current of the long

monopole antenna do not reinforce those radiated by original current, resulting in very poor radiation efficiency (Balanis, 1989). As a result, the antenna radiation pattern does not remain omnidirectional within the interested frequency range. In the conventional monopole antenna, the resonance frequencies ω_m correspond to the frequencies where the physical length L of the monopole is an odd multiple of quarter-wavelength. In other words, the antenna resonance frequencies are harmonics of the design frequency ω_1. However, omnidirectional radiation pattern distortion and low directivity are two major disadvantages associated with monopole resonating at higher order harmonics ($\omega_m > \omega_1$). In other words, conventional monopole antenna only radiates an omnidirectional radiation pattern at the design frequency ω_1. In order to have omnidirectional radiation pattern within the antenna bandwidth (ranging from f_L to f_U), the monopole length has to be less than $\lambda_U/2$, where λ_U is the free space wavelength at f_U. However, the antenna directivity decreases because of the significant reduction in the monopole length.

In this section, the use of AMCs to load a monopole antenna has been investigated. It is known that the current reversal, that occurs at frequencies much beyond the antenna natural frequency, disturbs the omnidirectional radiation pattern of the monopole antenna. The current distribution of the monopole antenna can be improved to a large extent by using PMC loading. To this aim, the CLLs are used to realize perfect magnetic conductor behavior.

2.1 PMC loaded monopole antenna

Due to the reverse current effects, the monopole radiation pattern does not remain omnidirectional at the second harmonic of the main resonant frequency (Balanis, 1989). In this section, a monopole antenna loaded with the PMC layer is proposed to increase omnidirectional radiation bandwidth. To make the concept more clear, three ideal models are simulated, all of which are partly covered by a very thin PMC shell, as shown in Fig. 1. As a reference, a conventional monopole antenna is also simulated for comparison. It has the same dimensions as the geometries in Fig. 1, except that the PMC cover is removed.

Fig. 2, shows the simulated reflection coefficient of the monopole antennas with and without the PMC cover. The resonant frequencies for case I and II are 18.5GHz and 24GHz, respectively, whereas the resonant frequency for case III remains the same as the conventional monopole antenna. For the conventional monopole antenna, distortion of the omnidirectional radiation pattern occurs at frequencies higher than 20GHz. This upper limit is indicated by dashed line in Fig. 2, and considered as an antenna length limitation.

Fig. 3, shows the radiation patterns of the monopole antennas with and without PMC cover when frequency varies from 12GHz to 30GHz in 1GHz increments. As revealed in the figure, when the monopole antenna is loaded with the PMC cover (case III), the antenna radiation pattern considerably improves as compared to that of the conventional monopole antenna, especially at the second harmonic of the main resonant frequency (29GHz).

Fig. 4, compares the simulated directivity of the monopole antennas with and without the PMC cover in the azimuth plane. As is evident from Fig. 4, the directivity curve for the case II is approximately flat while the antenna directivity for the case III significantly improves as compared to that of the conventional monopole antenna. For our discussion on the pattern modification, the results shown in Figs. 2 to 4, need to be considered simultaneously.
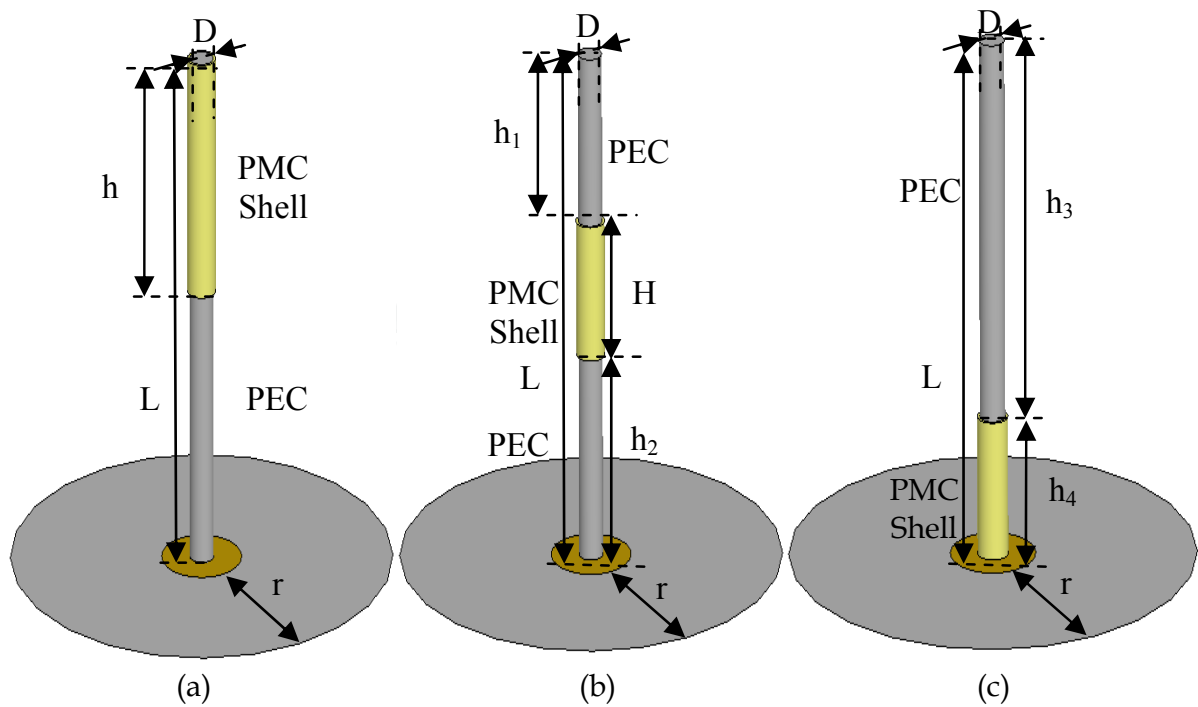
Fig. 1. Three ideal models of PMC loaded monopole antennas, (a) case I, (b) case II, and (c) case III: L=7.5mm, D=0.5mm and h=3.5mm, h_1=2.5mm, h_2=3mm, H=2mm, h_3=5.5mm, h_4=2mm, and r =4mm. From (Jafargholi et al., 2010), copyright © 2010 by the Institute of Electrical and Electronics Engineers (IEEE).
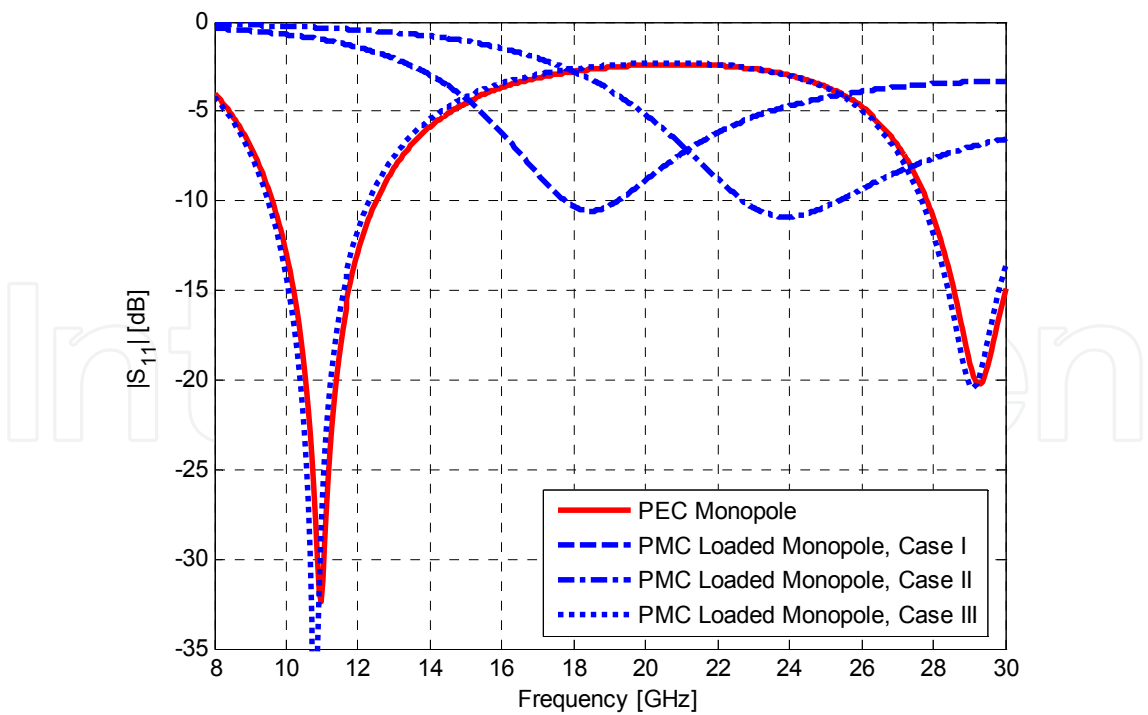

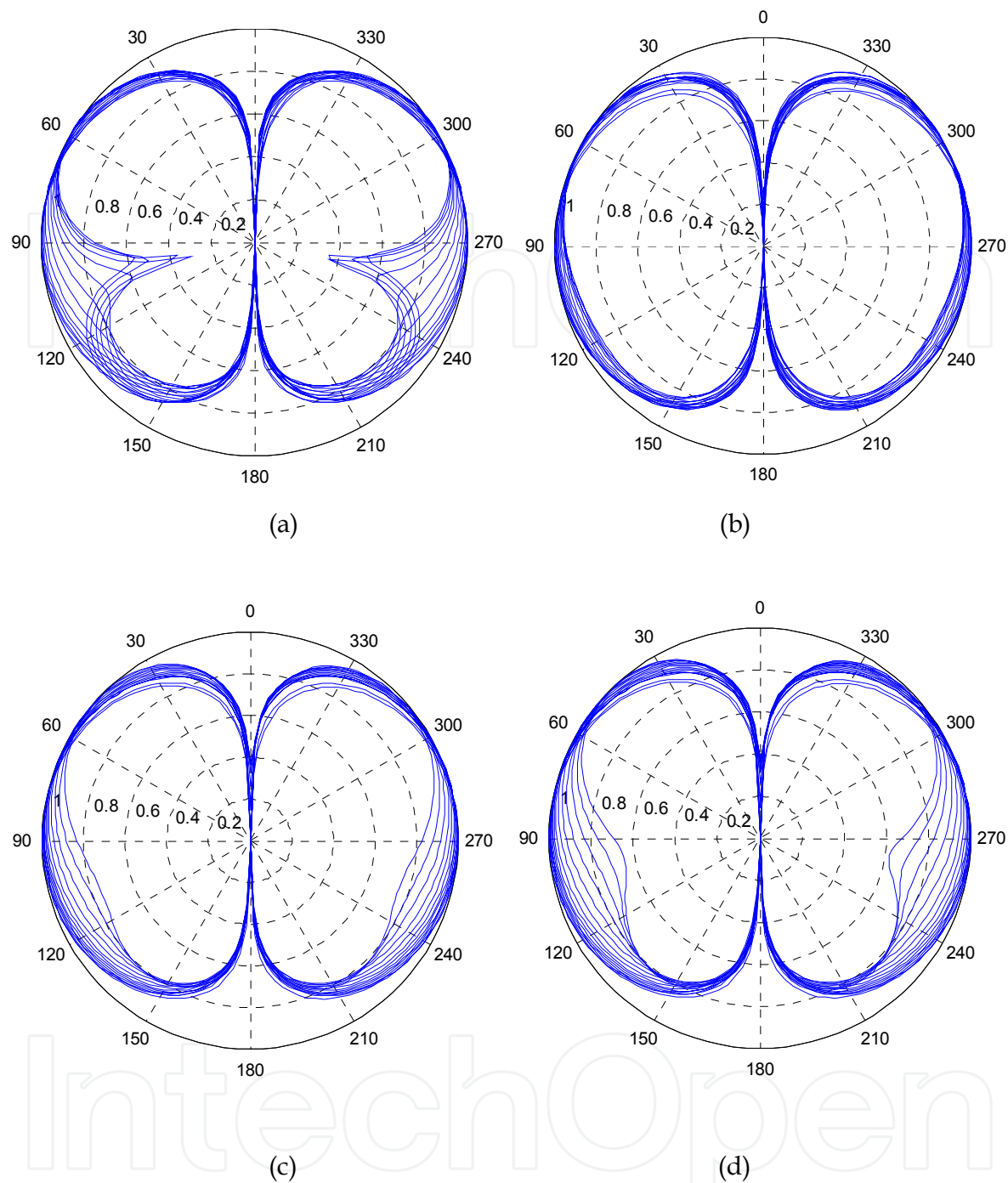Fig. 2. Reflection coefficient of monopole antennas with and without PMC cover. From (Jafargholi et al., 2010), copyright © 2010 by the Institute of Electrical and Electronics Engineers (IEEE).

Fig. 3. Normalized Radiation Patterns v.s. frequency (a) conventional monopole, (b) PMC loaded monopole (case I), (c) PMC loaded monopole (case II) , and (d) PMC loaded monopole (case III). From (Jafargholi et al., 2010), copyright © 2010 by the Institute of Electrical and Electronics Engineers (IEEE).

Consequently, the ideal model shown in Fig. 1 (c) (case III) is considered for the practical realization. It should be pointed out that we can always use a shorter monopole antenna to improve the omnidirectional radiation pattern. However, the prices we pay are the higher resonant frequency and lower directivity due to the significant reduction in the monopole length.
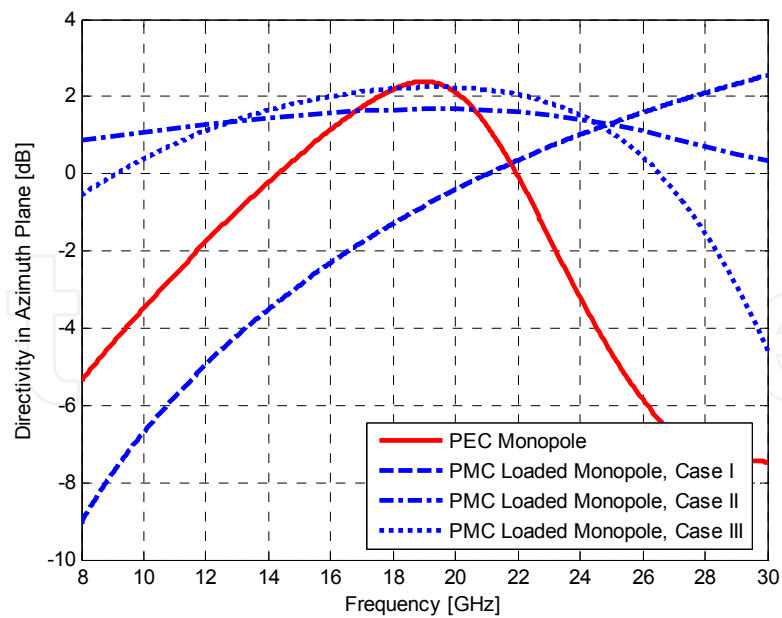
Fig. 4. Simulated directivity (maximum) of monopole antennas with and without PMC cover (on a finite ground plane) in azimuth plane. From (Jafargholi et al., 2010), copyright © 2010 by the Institute of Electrical and Electronics Engineers (IEEE).

2.2 CLL loaded monopole

In the previous section, it was revealed that the suppression of phase reversal by incorporating PMC cover has led to the improved radiation pattern, especially at the second harmonic of the main resonant frequency. In this section, the capacitively loaded loops (CLLs) are used to realize an artificial PMC (Erentok et al., 2005). Fig. 5 shows a CLL loaded monopole antenna together with the basic unit cell of the CLL structure. The finite two-CLL-deep metamaterial AMC cover was designed separately (without the ground plane) to operate at around 26GHz. The CLL dimensions were then optimized to obtain good radiation patterns. The total number of the CLL elements is 44 and the separation between the CLL elements is 0.5mm.
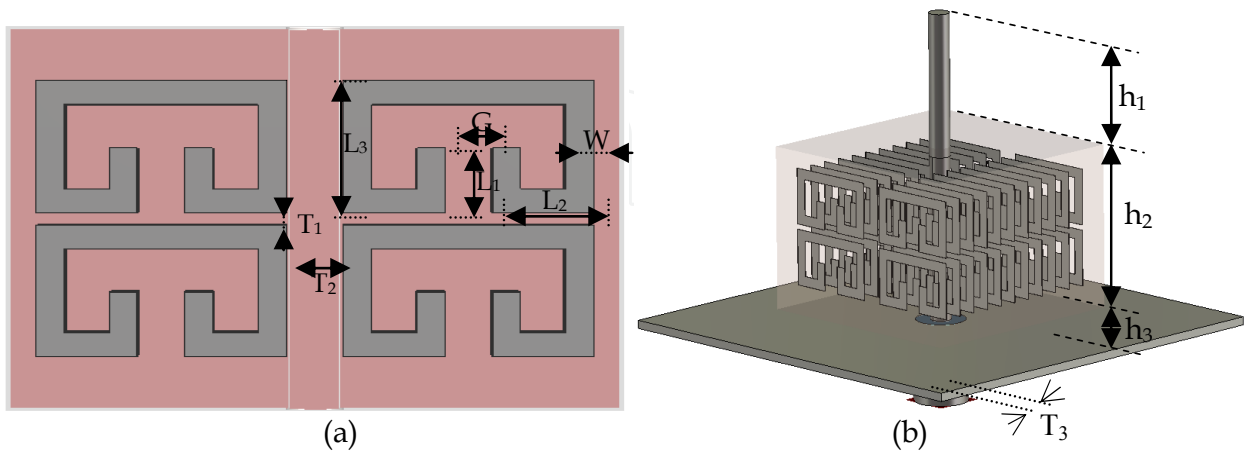

(a)   (b)

Fig. 5. A schematic view of (a) CLL unit cell: L_1=0.67mm, L_2=0.89mm, L_3=1.37mm, W= 0.247mm, G=0.411mm, T_1= 0.13mm, T_2= 0.5mm, and (b) CLL loaded monopole antenna on a finite ground plane: h_1= 3.25mm, h_2 =4mm, h_3=0.25mm, T_3=0.45mm. From (Jafargholi et al., 2010)], copyright © 2010 by the Institute of Electrical and Electronics Engineers (IEEE).

Fig. 6 shows a comparison between the reflection coefficients of the CLL loaded and unloaded monopole antennas of 7.5mm length. Furthermore, Fig. 7 shows the surface current densities on the CLL loaded and unloaded monopole antennas. It can be seen that the current in the CLL loaded region is the superposition of two currents oriented in opposite directions. However, the surface current caused by CLL cells is dominant, and thus the current in all parts of the monopole has the same phase. To more understand the operation mechanism of the CLL loaded monopole antenna, we assume that the monopole antenna is surrounded by CLL cells, where the current direction of the monopole is reversed. Fig. 8, conceptually explains the distribution of the surface current density on the CLL loaded monopole antenna.
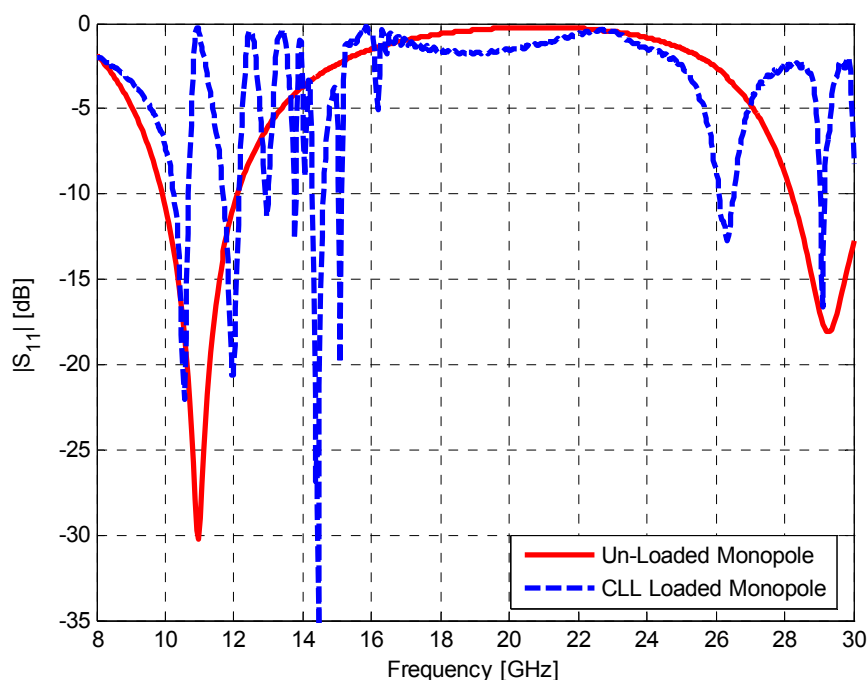

Fig. 6. Simulated reflection coefficient of the CLL loaded and unloaded monopole antennas. From (Jafargholi et al., 2010), copyright © 2010 by the Institute of Electrical and Electronics Engineers (IEEE).

A rigorous explanation must consider the complex interactions between the monopole and the CLL structure, such as the effects of the finite dimensions of the CLL structure on the current distribution. Consequently, full wave analysis methods have to be used in the antenna designs. However, to simplify the analysis, one can assume that the transverse dimensions of the CLL loaded region are infinite in extent.

Based on image theorem, when an electric current is vertical to a PMC (PEC) region, the current image has the reversed (same) direction. For the current at the bottom of the monopole flowing into the CLL loaded region, the CLL loaded region acts as a PMC cover (Erentok et al., 2005). Consequently, the direction of the image current is opposite to that of the original current, as shown in Fig. 8.
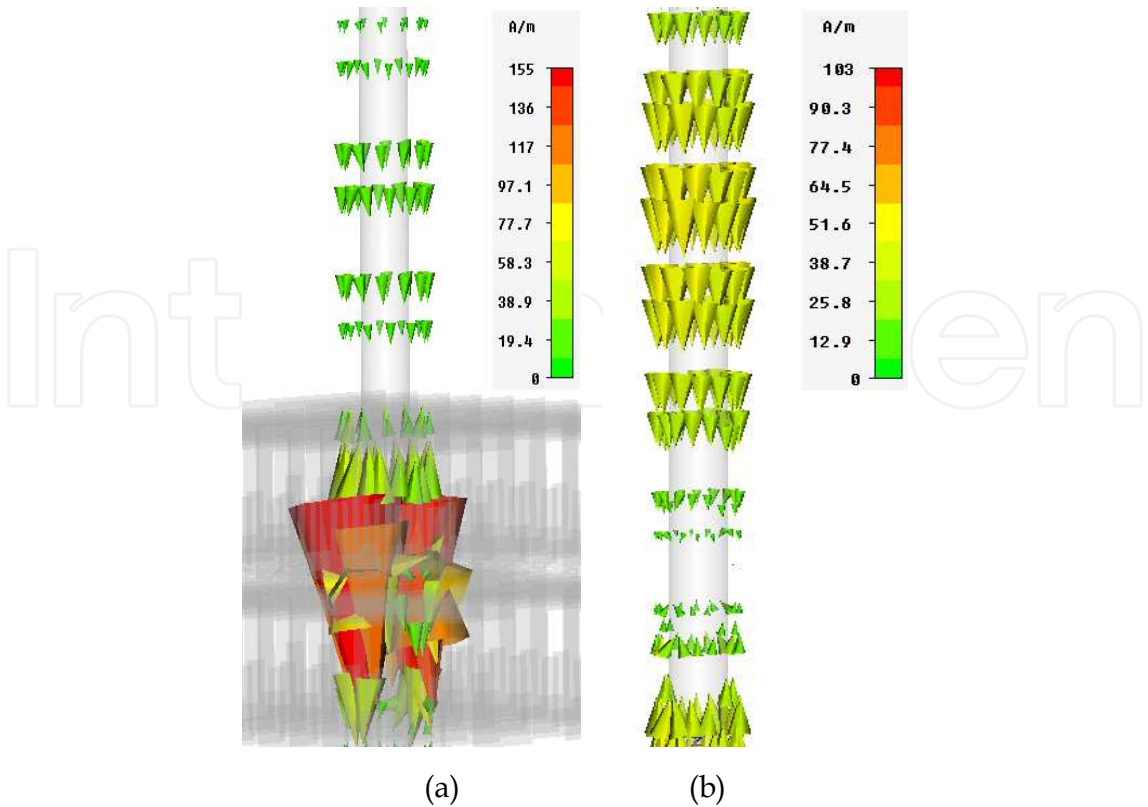
Fig. 7. Surface current densities on the (a) CLL loaded monopole and (b) unloaded monopole at *f*= 25GHz. From (Jafargholi et al., 2010), copyright © 2010 by the Institute of Electrical and Electronics Engineers (IEEE).
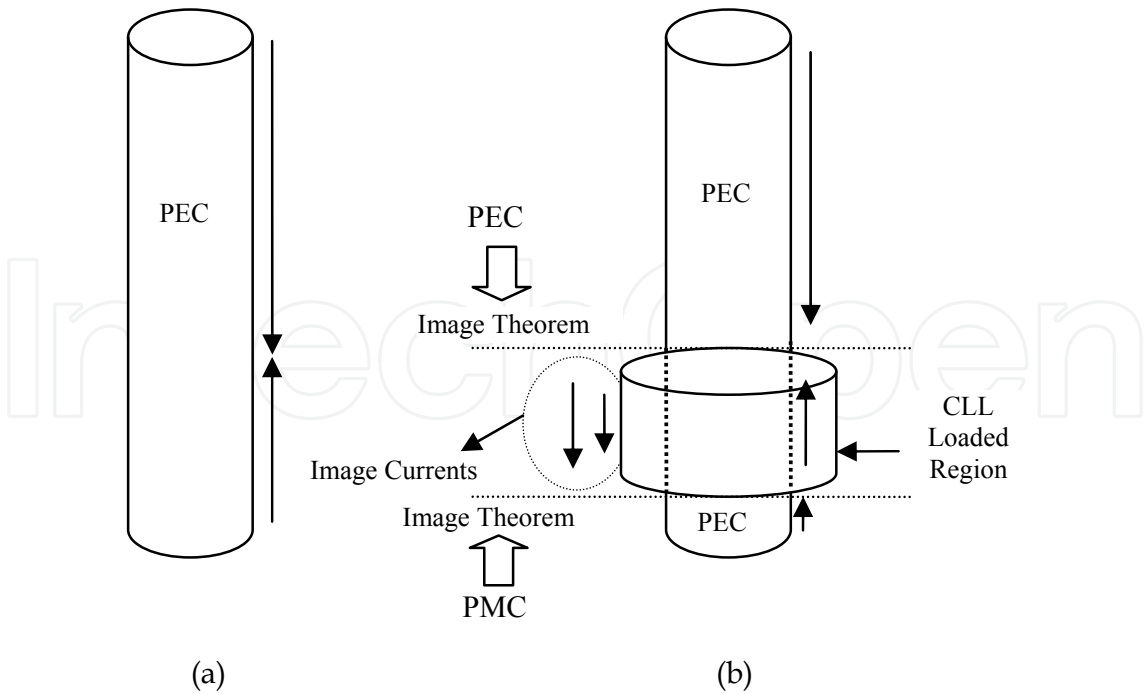

Fig. 8. Conceptual schematics of the (a) conventional and (b) PMC-loaded monopoles. From (Jafargholi et al., 2010)], copyright © 2010 by the Institute of Electrical and Electronics Engineers (IEEE).

In contrast, for the current at the top of monopole flowing into the CLL loaded region, the CLL loaded region acts as an artificial electric conductor (AEC) (Erentok et al., 2005), and thus the image current in the CLL loaded region has the same direction as the original current. The total surface current in the CLL loaded region is obtained as the sum of the two image currents and original current. Consequently, the current phase of the CLL loaded monopole antenna remains unchanged throughout the antenna, as shown in Fig. 8. The radiation patterns of the conventional and CLL loaded monopole antennas on a finite ground plane are shown in Figs. 9 and 10, respectively. As can be seen, when the monopole antenna is loaded with the CLL structure, the radiation patterns improve significantly, especially at the second harmonic (26GHz, 29GHz, and 30GHz) of the main resonant frequency where antenna is matched well.

Also, the antenna radiation efficiency is reasonably high over a wide frequency window, despite the material loss in copper and the CLL metamaterial features. Although, simulation results confirm the modification of the antenna radiation patterns at frequencies up to around 30GHz, the antenna reflection coefficient needs to be modified by impedance matching techniques, especially at frequencies far from the antenna resonant frequencies (Erentok et al., 2008). The simulated gains of the CLL loaded and unloaded monopole antennas in azimuth plane are compared in Fig. 11. As compared to the conventional monopole antenna, the gain of the CLL loaded monopole antenna significantly increases, especially at the higher frequencies. These comparisons demonstrate the unique capability of the AMCs to improve the antenna radiation bandwidth. It is worth noting that the antenna radiation patterns are not completely symmetric in the frequency band from 12GHz to 30GHz because of the asymmetric geometry.
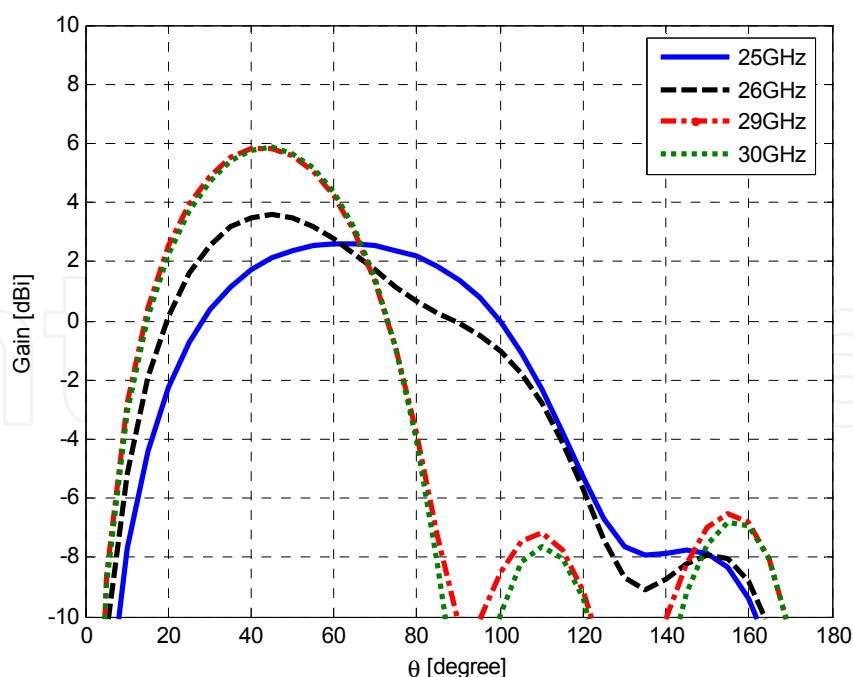

Fig. 9. Radiation patterns of the conventional monopole antenna versus frequency at φ=0˚. From (Jafargholi et al., 2010), copyright © 2010 by the Institute of Electrical and Electronics Engineers (IEEE).

Fig. 10. Radiation patterns of the CLL loaded monopole antenna versus frequency at $\varphi=0^0$. From (Jafargholi et al., 2010), copyright © 2010 by the Institute of Electrical and Electronics Engineers (IEEE).
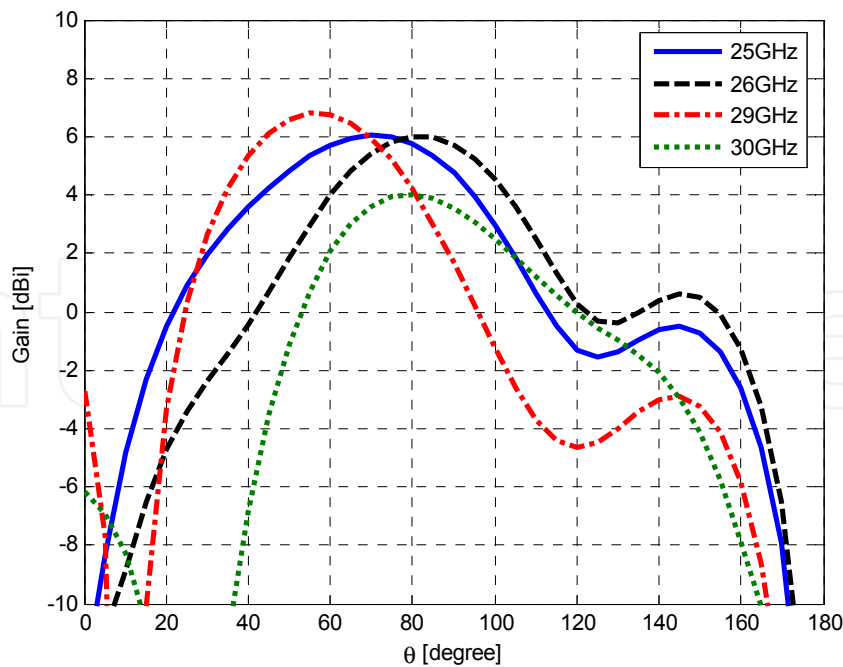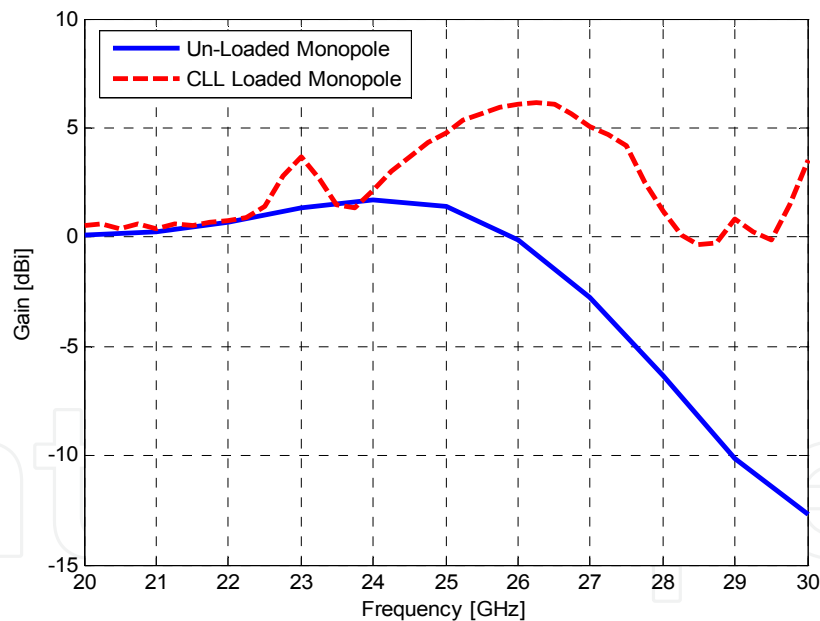

Fig. 11. Comparison of the maximum gains of the monopole antennas with and without CLL covers (on a finite ground plane) in the azimuth plane. From (Jafargholi et al., 2010), copyright © 2010 by the Institute of Electrical and Electronics Engineers (IEEE).

2.3 Pattern modification of dipole antenna

Dipole antennas are preferable in modern wireless communication systems, especially their printed types, due to their low profile, light weight and low fabrication cost as well as their compatibility with microwave and millimeter wave circuits. It was revealed in (Erentok et

al., 2007; Erentok et al., 2008) that an efficient and electrically small magnetic based antenna can be realized by adding a planar interdigitated CLL element to a rectangular semi-loop antenna, which is coaxially-fed through a finite ground plane. The performance of a printed dipole antenna near a 3D-CLL block has been also examined in (Zhu et al., 2010). Recently, the use of TL-MTM to load antennas has been investigated in (Antoniades et al., 2009; Zhu et al., 2009). A miniaturized printed dipole loaded with left-handed transmission lines is also proposed in (Iizuka et al., 2006; Iizuka et al., 2007).

However, it is known that the conventional dipole antenna only radiates an omni-directional radiation pattern at the design frequency ω_1. As described in the previous section, the suppression of phase reversal by incorporating PMC cover has led to the improved radiation pattern (Jafargholi et al., 2010). This section is focused on the pattern modification of the wire dipole antenna using artificial magnetic conductors.

Fig. 12, shows a CLL loaded dipole antenna. The finite two-CLL-deep metamaterial Artificial Magnetic Conductor (AMC) cover was designed separately to operate at around 27GHz. The CLL dimensions were then optimized and placed optimally on both dipole arms to obtain good radiation patterns. The total number of the CLL elements is 88 (4×11×2) which symmetrically coupled to dipole antenna arms. The separation between the CLL elements is also fixed at 0.5mm.

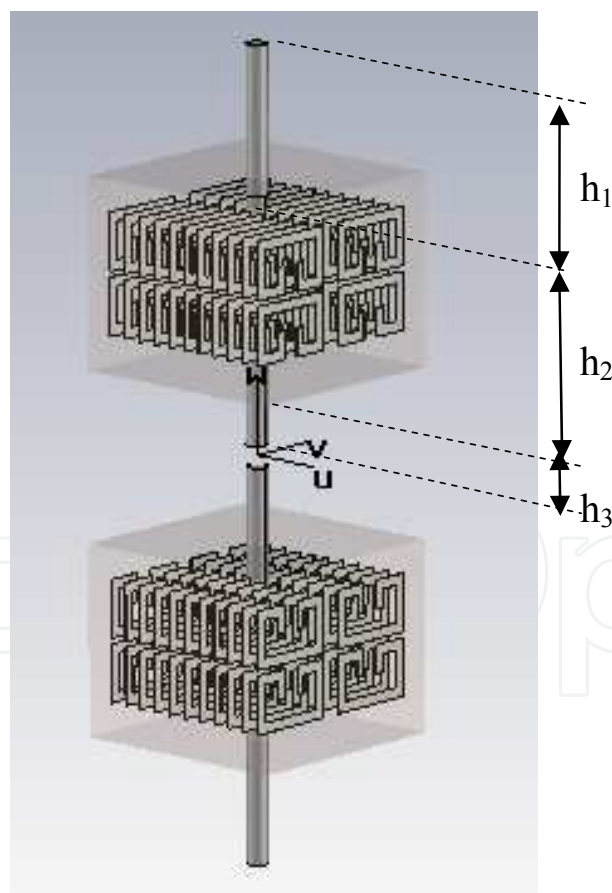Fig. 12. A schematic view of CLL loaded dipole antenna, unit cell parameters (See Fig. 5a): L_1=0.67mm, L_2=0.89mm, L_3=1.37mm, W= 0.247mm, G=0.411mm, T_1= 0.13mm, T_2= 0.5mm, h_1= 3.25mm, h_2 =4mm, h_3 =2mm, and antenna feed gap = 0.5mm, and length of dipole antenna =19mm.

Fig. 13, shows a comparison between the reflection coefficient and input impedance of CLL loaded and unloaded wire dipole antennas of 19mm length. It was revealed in (Jafargholi et al., 2010) that ideally the dipole antenna input impedance does not change significantly by using AMC loading. However, here, the input impedance for the realized CLL loaded dipole changes due to the existence of the CLL resonance and the interaction between the CLL elements and the dipole antenna.
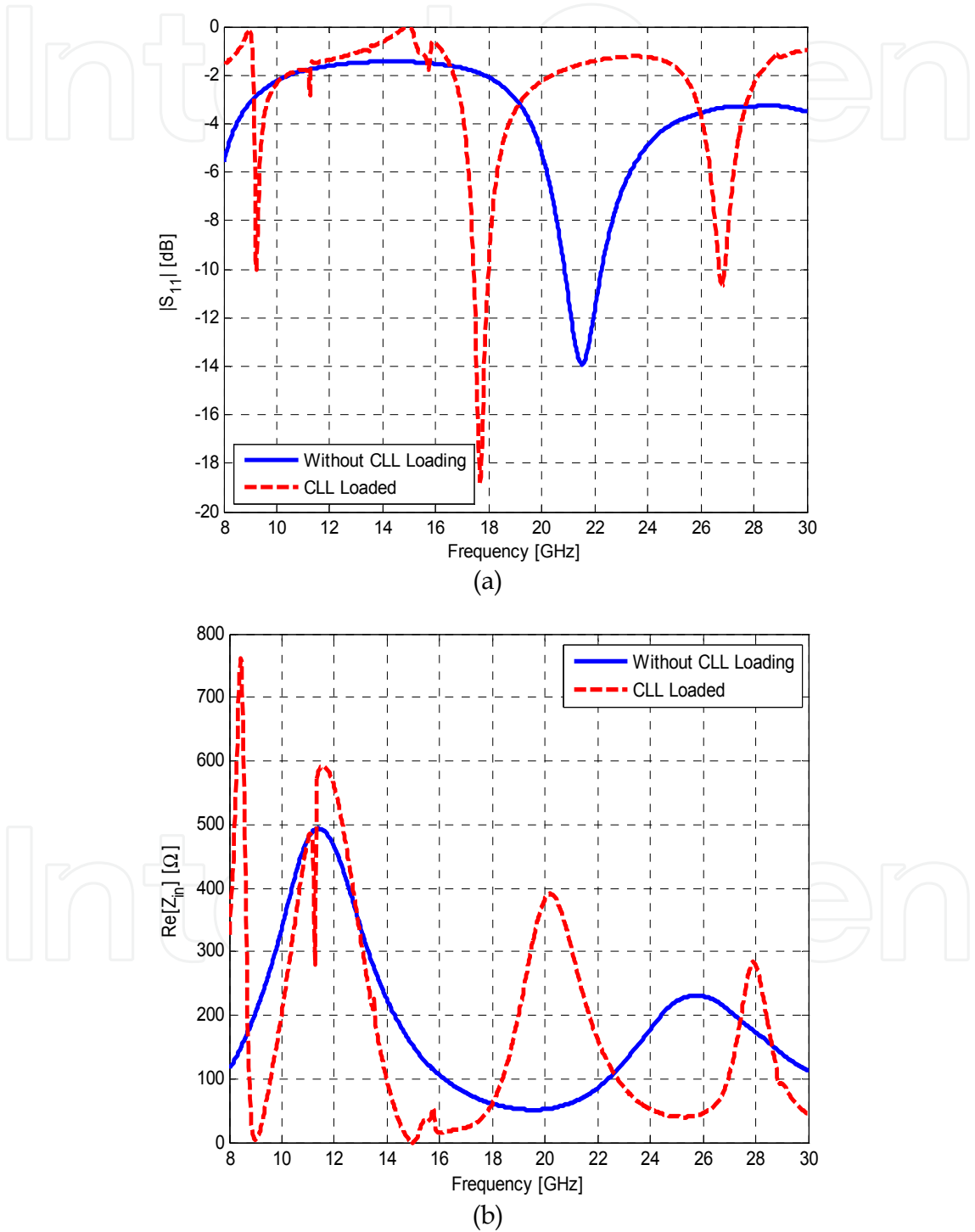

(a)

(b)

Fig. 13. (a) simulated reflection coefficient, and (b) Input Impedance of the CLL loaded and unloaded wire dipole antennas.

Fig. 14, shows the surface current densities on the CLL loaded and unloaded dipole antennas. As can be seen, the current in the CLL loaded region is the superposition of two currents oriented in opposite directions. However, the surface current caused by CLL cells is dominant, and thus the current in all parts of the dipole has the same phase. To clarify the operation mechanism of the CLL loaded dipole antenna. We assume that dipole antenna is surrounded by CLL cells, where the current direction of the dipole is reversed.
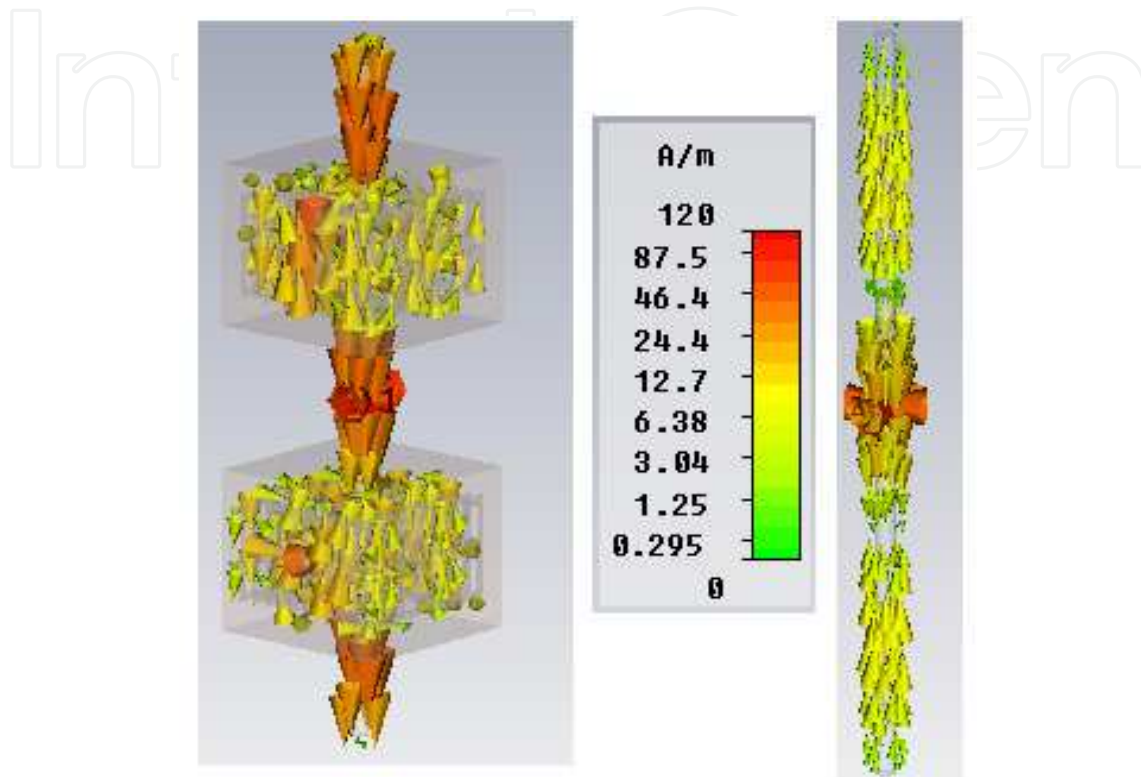
Fig. 14. Surface current densities on the CLL loaded dipole (left) and unloaded dipole (right) at f= 27GHz.

Fig. 15, conceptually explains the distribution of the surface current density on the CLL loaded dipole antenna. However, one must consider the complex interactions between the dipole arms and the CLL structures, such as the effects of the finite dimensions of the CLL structures on the current distribution. Consequently, full wave analysis methods have to be used in the antenna designs. However, to simplify the analysis, one can assume that the transverse dimensions of CLL loaded region are infinite in extent. Thus, as previous section, one can explain the concept based on the image theorem, i.e., when an electric current is vertical to a PMC (PEC) region, the current image has the reversed (same) direction.

For the current at the bottom of the dipole flowing into the CLL loaded region, the CLL loaded region acts as a PMC cover (Erentok et al., 2005). At the result, the direction of the image current is opposite to that of the original current, as shown in Fig. 15. In contrast, for the current at the top of dipole flowing into the CLL loaded region, the CLL loaded region acts as an AEC (Erentok et al., 2005), and thus the image current in the CLL loaded region has the same direction as the original current. The total surface current in the CLL loaded region is obtained as the sum of the two image currents and original current. At the result, the current phase of the CLL loaded dipole antenna remains unchanged through the antenna, as shown in Fig. 15.
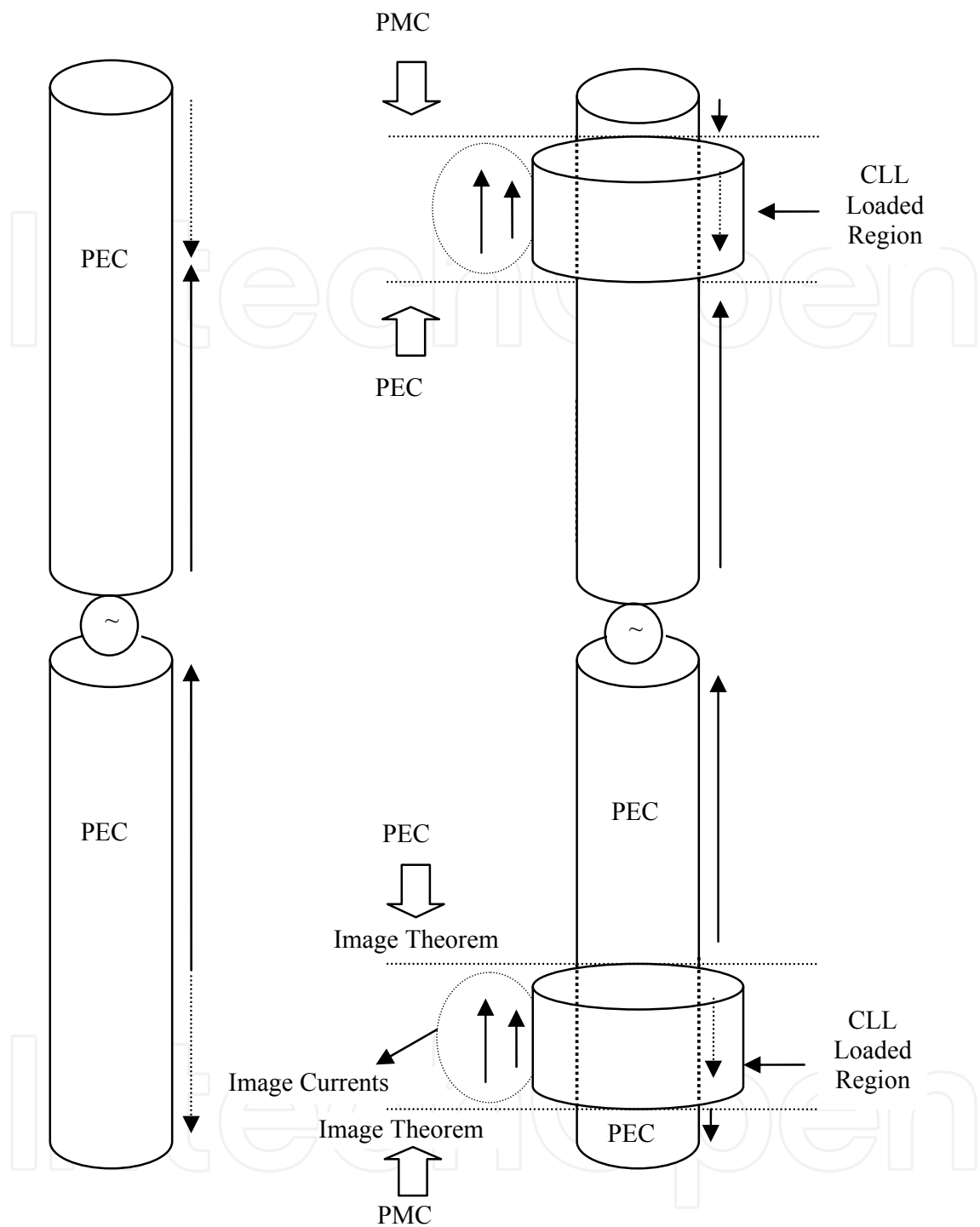
Fig. 15. Conceptual schematics of the conventional (left) and CLL loaded dipole (right).

The radiation patterns of the conventional and CLL loaded dipole antennas are also shown in Fig. 16, respectively. As can be seen, when the dipole antenna is loaded with CLL structure, the radiation patterns improve significantly, especially at the second harmonic (27GHz) of the main resonant frequency where antenna is matched well. The Simulation shows that above 20dB gain enhancement has been achieved in azimuth plane using CLL loading technique.

(a)

(b)
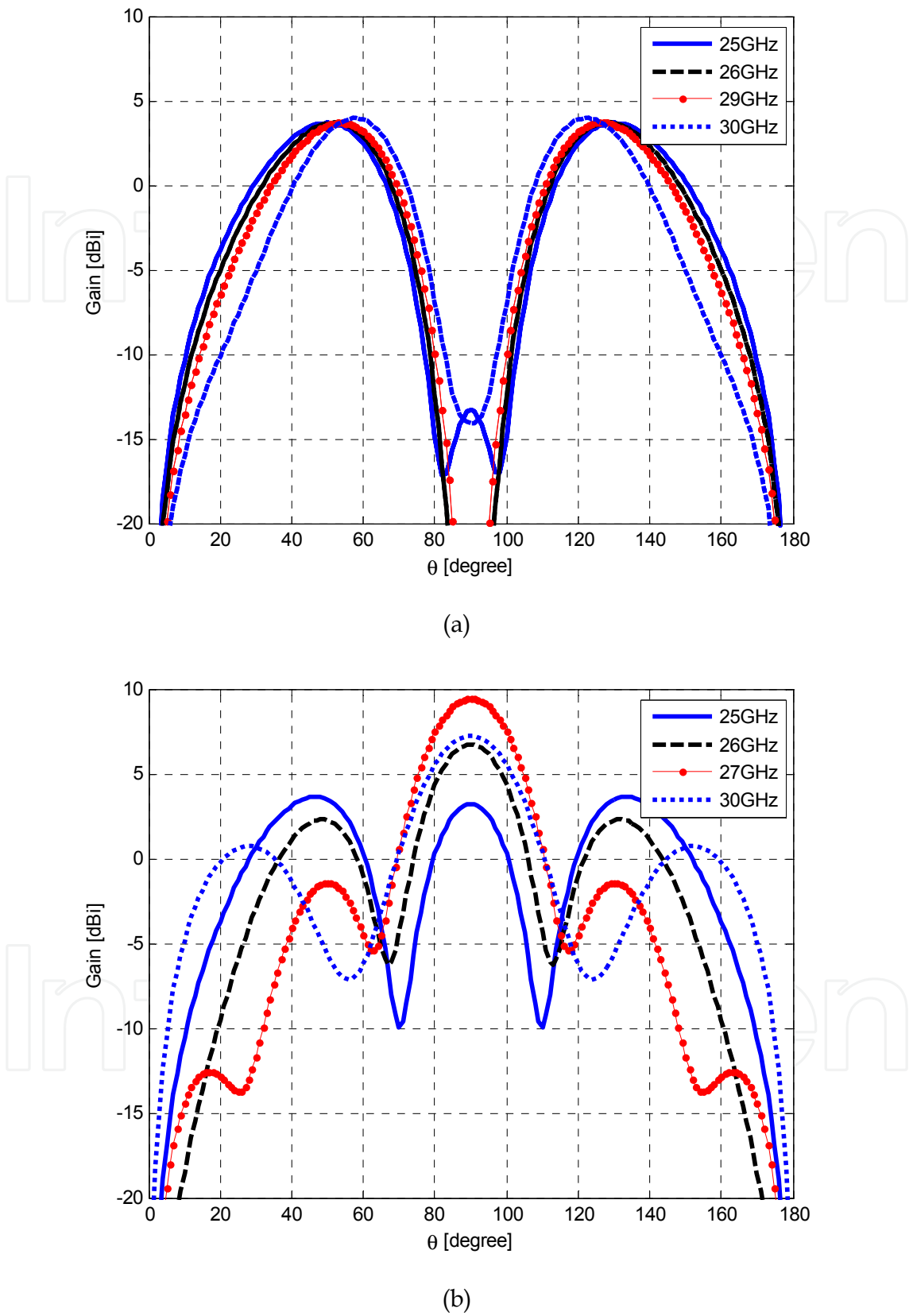
Fig. 16. Radiation patterns of (a) conventional wire dipole antenna, and (b) the CLL loaded dipole antenna versus frequency at $\varphi=0^0$.

2.4 Compact dual band loaded dipole antenna, incorporating artificial magnetic conductors

The interesting features of printed dipole antennas make it possible for them to be conformal with installation platforms such as automobiles and vessels, without affecting the aerodynamic or mechanical properties of the vehicles. In the recent years, due to unique electromagnetic properties, metamaterials have been widely considered in monopole and dipole antennas to improve their performance. However, the left-handed dipole antennas (Zhu et al., 2009; Iizuka et al., 2006; Iizuka et al., 2007), albeit compact, suffer from the losses in the loading components, namely, interdigitated capacitors and meander inductors, resulting in a very low gain.

In this section, we propose a new dual band printed dipole antenna in that CLL elements as reactive loads are placed close to the edge of the dipole. The losses associated with the CLL elements are very low in the frequency range of interest, resulting in both the acceptable gain and radiation pattern. When the CLL elements are incorporated, the resonant behavior of the unloaded printed dipole antenna changes. As a result, a new resonance is appeared with the frequency determined by the CLL dimensions. In fact, the CLL element can be easily described as an LC resonant circuit in which the resonant frequency is mainly determined by the loop inductance and the gap capacitor. It is worth noting that the resonant behavior of the CLL element starts to appear at a frequency in which the free space wavelength is much larger than its size. However, the second resonant frequency of the CLL-loaded dipole occurs at a frequency higher than the main resonant frequency of the unloaded dipole. To further reduce the second resonant frequency without increasing the area occupied by the antenna, chip capacitors are incorporated in the CLL elements. The chip capacitor provides a tuning capability of the second resonant frequency. Thus the frequency ratio between these two frequencies can be readily controlled by incorporating different chip capacitors into the capacitive gaps of the CLL elements. It is worthwhile to point out here that the CLL elements integrated with chip capacitors miniaturize the size of the printed dipole antenna.

The reason is that when the chip capacitor value is increased, the CLL resonant frequency decreases, and thus the second resonant frequency of the dipole shifts down to a lower frequency. The proposed dual band CLL loaded dipole antenna radiates effectively at both resonant frequencies with good return losses and gains as well as acceptable omnidirectional radiation patterns. The high-frequency structure simulator (Ansoft HFSS) is adopted for the simulations.

2.4.1 Dual band printed dipole antenna

In order to test the proposed approach, double-sided printed dipole antenna is loaded by CLL elements. Fig. 17, shows the CLL-loaded printed dipole antenna together with the CLL element. The dipole and CLL elements are printed on a FR4 substrate with a thickness of 0.8mm and a dielectric constant of 4.4 to reduce the cost of the antenna and to make it more rigid in construction. The CLL-loaded printed dipole has also been optimized to realize better performance. The optimized parameters of the proposed CLL-loaded dipole antenna are labeled in the Fig. 17. A prototype of the proposed CLL-loaded printed dipole is fabricated to validate the simulation results.

A photograph of the fabricated printed dipole antenna is shown in Fig. 18. Fig. 19, shows the reflection coefficient of the proposed dual band printed dipole antenna as well as the unloaded dipole antenna. As can be seen, the agreement between the simulation and measurement results is reasonably good. It is observed that when the CLL elements are added, two resonance frequencies become distinguishable from each other and thus two nulls are clearly observed in the reflection coefficient curve. The unloaded dipole antenna resonates at around 2.75GHz. In contrast, the fabricated CLL-loaded dipole resonates at 2.15 and 4.45GHz, as shown in Fig. 19. The lower resonant frequency corresponds to that of the original printed dipole and remains approximately unchanged while the higher resonant frequency is mainly due to the CLL loading. To further understand the performance of the printed dipole antenna near the CLL elements, Fig. 20, shows the magnitude of the S-parameters versus frequency for the CLL-based metamaterial.
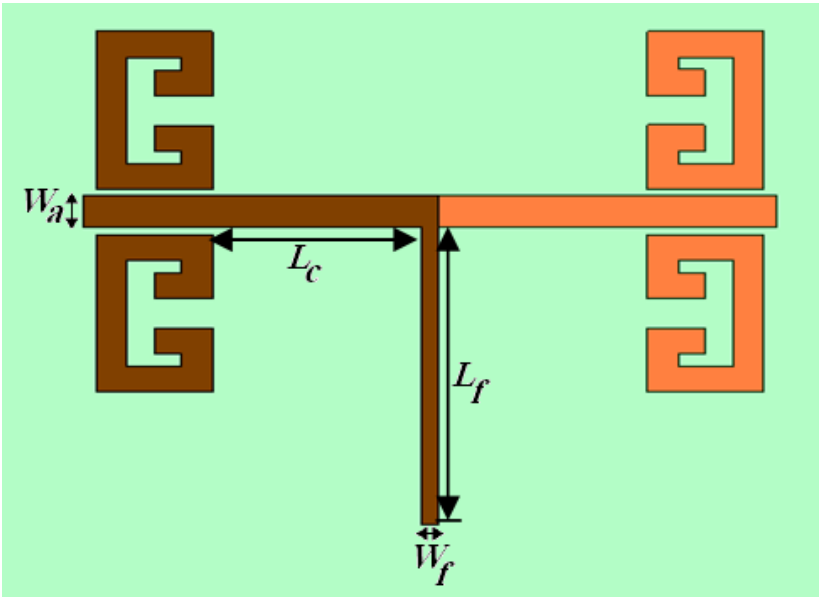
Fig. 17. Geometry of a CLL-loaded printed dipole antenna, L_f=23mm, L_c=13.67mm, W_f=1mm, W_a=2.5mm, L_1=3.73mm, L_2=4.95mm, L_3=7.62mm, G=2.28mm, W=2mm. From (Jafargholi et al., 2010), copyright © 2010 by Praise Worthy Prize, S. r. l.
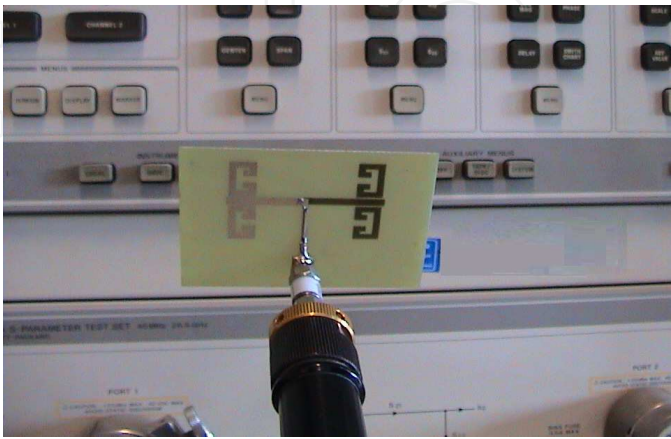

Fig. 18. Photograph of a fabricated CLL-loaded printed dipole antenna. From (Jafargholi et al., 2010), copyright © 2010 by Praise Worthy Prize, S. r. l.
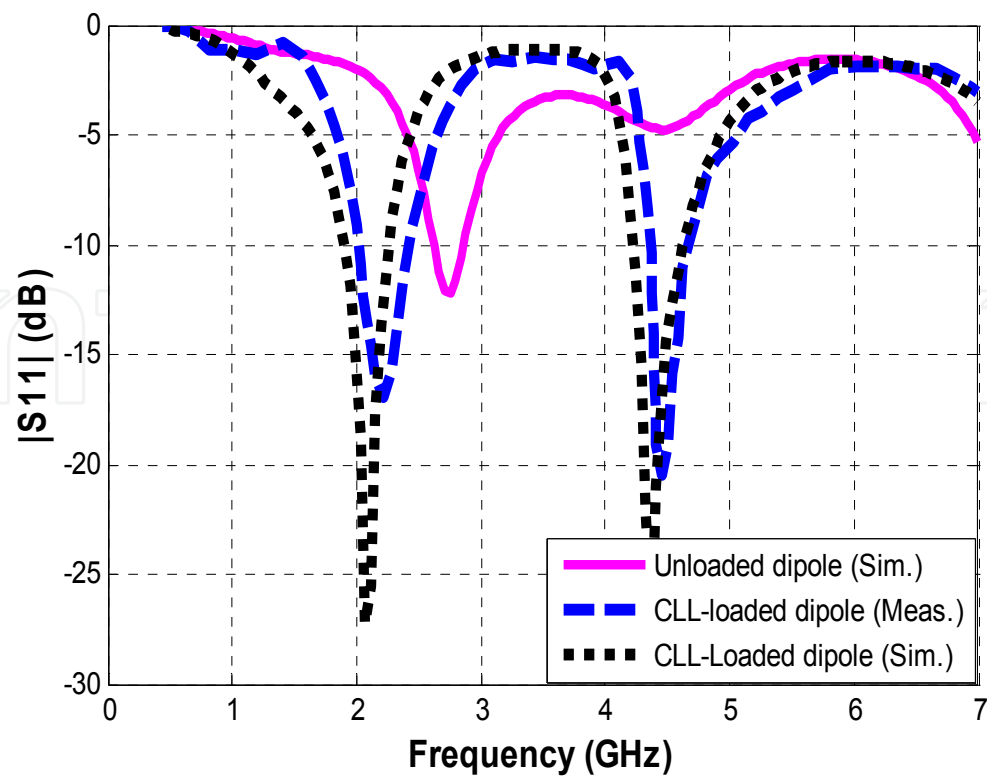
Fig. 19. Reflection coefficient comparison between the CLL-loaded and unloaded printed dipole antenna. From (Jafargholi et al., 2010), copyright © 2010 by Praise Worthy Prize, S. r. l.
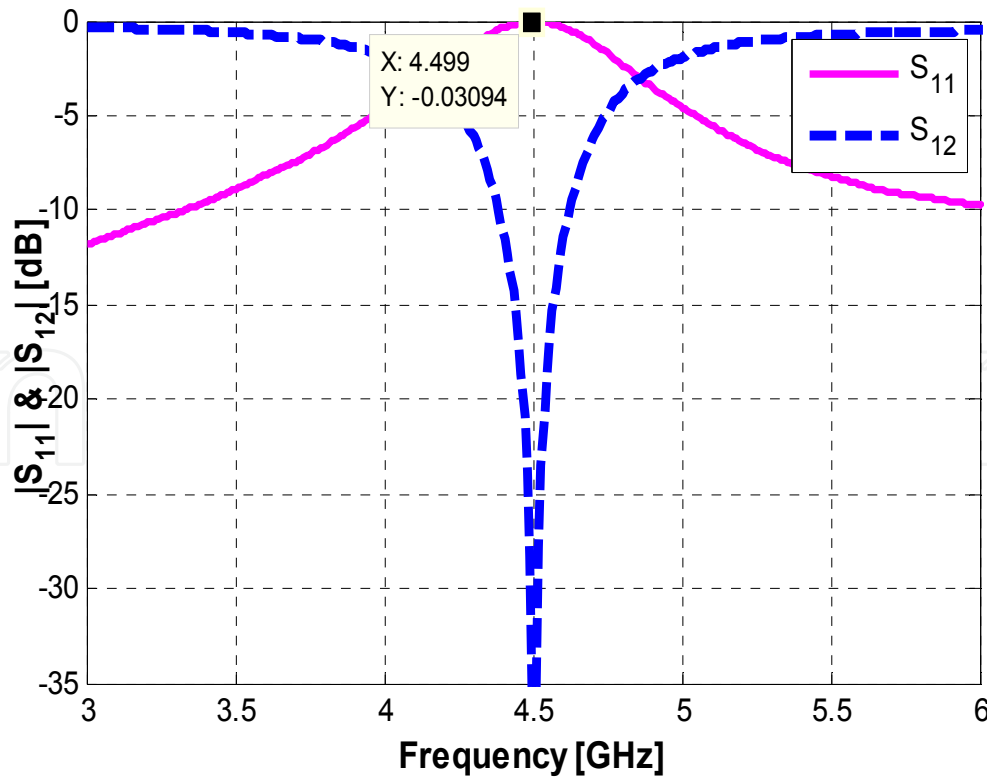

Fig. 20. Magnitude of the S-parameters versus frequency for the CLL-based metamaterial. From (Jafargholi et al., 2010), copyright © 2010 by Praise Worthy Prize, S. r. l.

It is observed that the CLL element effectively resonates at around 4.5GHz with small loss. This frequency coincides with the second resonant frequency of the CLL-loaded printed dipole (see Fig. 19). The radiation patterns of the proposed dual band printed dipole are measured at the resonant frequencies of 2.15 and 4.45GHz. Fig. 21, shows the measured and simulated E-plane radiation patterns at first and second resonant frequencies. The antenna gains at first and second resonant frequencies are 1.8dB, and 3.9dB, respectively. As a result, the losses introduced by the CLL elements are significantly low in the frequency range of interest. In other words, the proposed dual band dipole antenna has acceptable performance in both gain and radiation pattern.
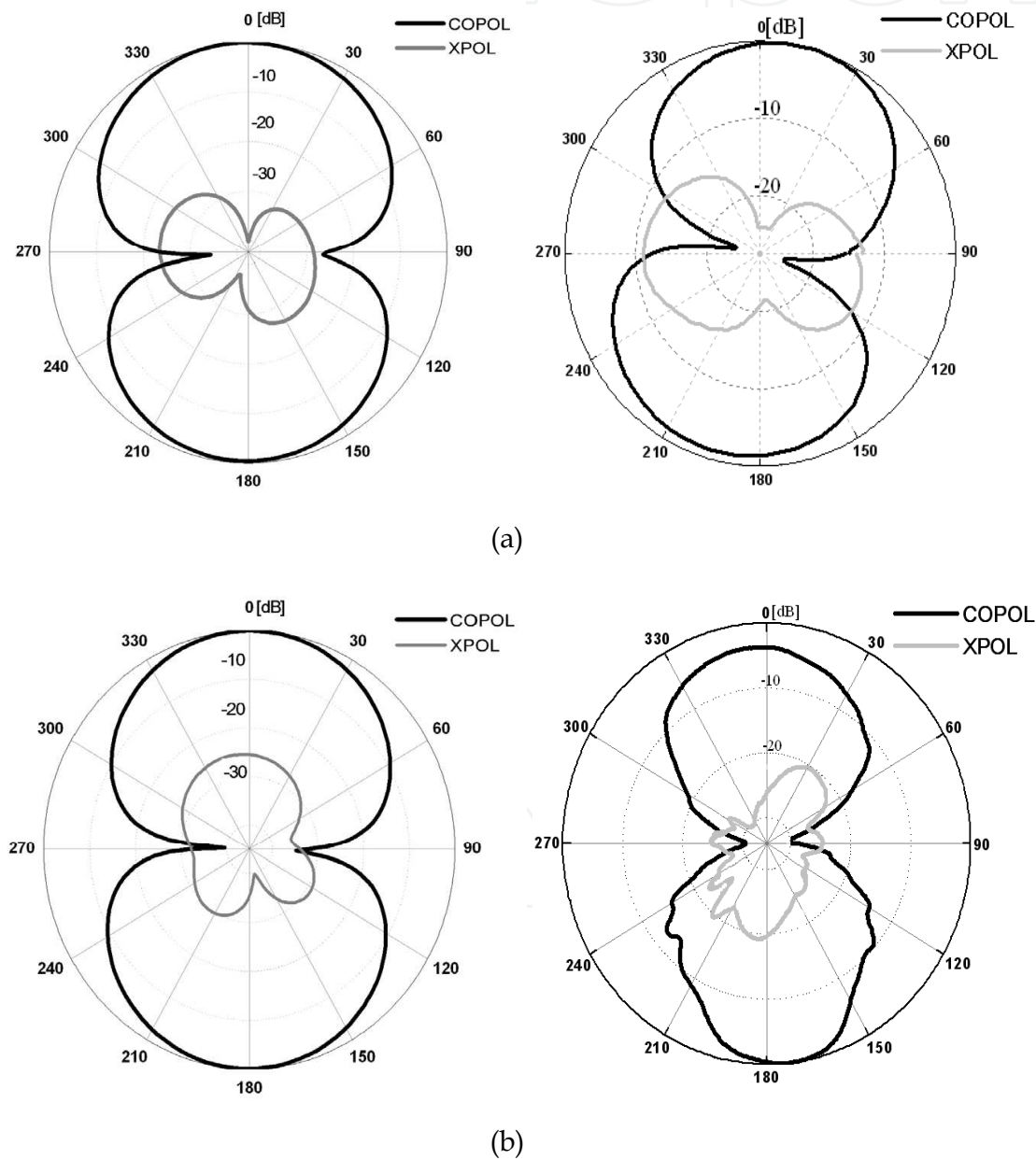

(a)

(b)

Fig. 21. E-plane radiation patterns of the CLL-loaded dipole antenna at (a) 2.15GHz, and (b) 4.45GHz. (Right hand figures are measurements). From (Jafargholi et al., 2010), copyright © 2010 by Praise Worthy Prize, S. r. l.

2.4.2 Miniaturized CLL-loaded printed dipole antenna incorporating chip capacitors

In principle, the size reduction can be arbitrarily achieved if it would be feasible to fabricate a proper metamaterial element that has a negative permeability at a frequency lower than the natural resonance frequency of the corresponding unloaded dipole antenna. For a metamaterial comprised of resonant CLL elements, this can be achieved by capacitive loading of the CLL elements. To verify and confirm the proposed approach, a prototype of a CLL-loaded dipole antenna, in which each CLL ring is loaded with a 0.68pF chip capacitor, is fabricated and measured.

A photograph of the fabricated miniaturized printed dipole antenna is shown in Fig. 22. The magnitude of the S-parameters for the CLL-based metamaterial loaded with a 0.68PF chip capacitor is shown in Fig. 23. As can be seen, the resonant frequency of the CLL element shifts down to 1.33GHz by incorporating 0.68PF chip capacitor (see Figs. 21, 23). In order to meet the specification of both the ISM system and mobile communication, the miniaturized printed dipole should radiate linearly polarized waves at 1.8GHz and 2.45GHz.
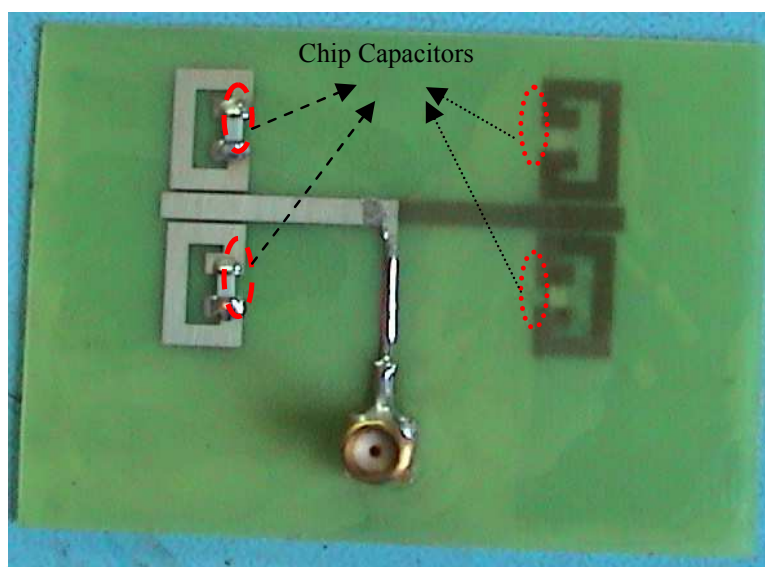

Fig. 22. Photograph of the miniaturized CLL-loaded printed dipole antenna (incorporating 0.68pF chip capacitors). From (Jafargholi et al., 2010), copyright © 2010 by Praise Worthy Prize, S. r. l.

Fig. 24, compares the measured and simulated reflection coefficient of the proposed miniaturized CLL-loaded printed dipole antenna. As can be seen, the second resonant frequency of the proposed CLL-loaded dipole of Section 1-2, considerably shifts down to a lower frequency by incorporating chip capacitors. The resonant frequencies of the proposed miniaturized CLL-loaded printed dipole are lower than the main resonant frequency of the unloaded dipole antenna. It should be pointed out that the antenna radiation patterns at both resonant frequencies are quite similar to that of a half wavelength dipole, as shown in Fig. 25. The antenna gains at first and second resonant frequencies are 0.62dB, and 2.26dB, respectively.
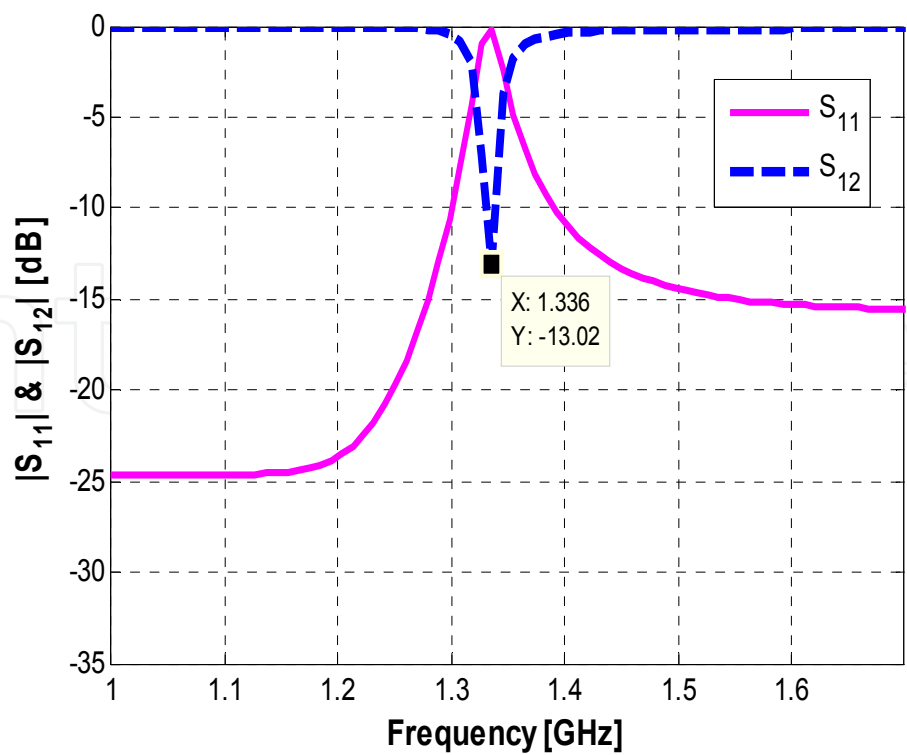
Fig. 23. Magnitude of the S-parameters versus frequency for the CLL based metamaterial loaded with a 0.68PF chip capacitor. From (Jafargholi et al., 2010), copyright © 2010 by Praise Worthy Prize, S. r. l.
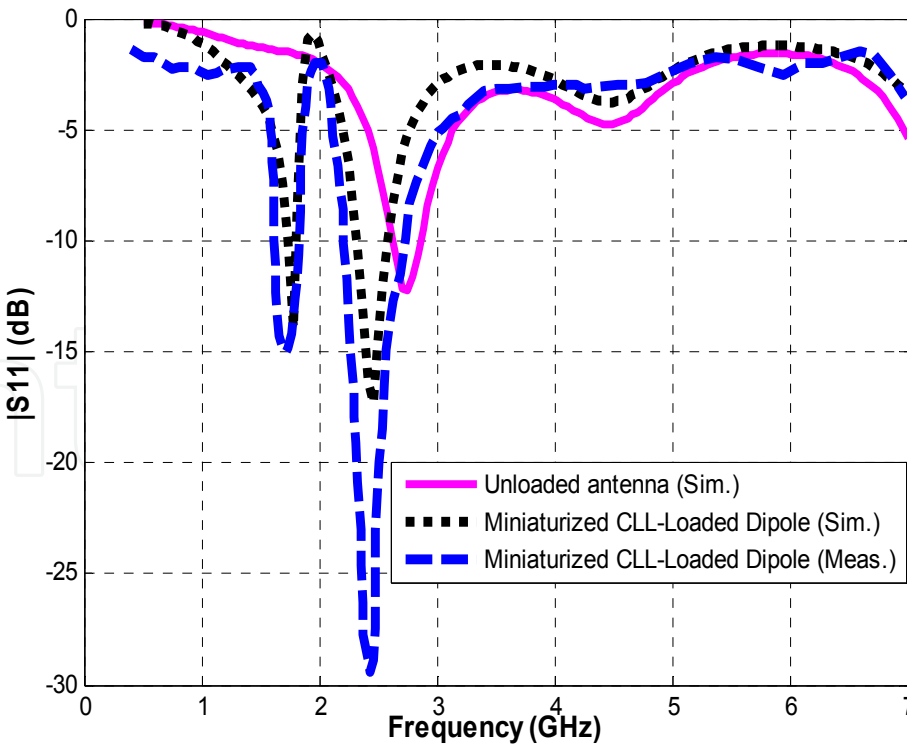

Fig. 24. Measured and simulated reflection coefficient of the miniaturized CLL-loaded printed dipole antenna, as compared to that of the unloaded printed dipole. From (Jafargholi et al., 2010), copyright © 2010 by Praise Worthy Prize, S. r. l.
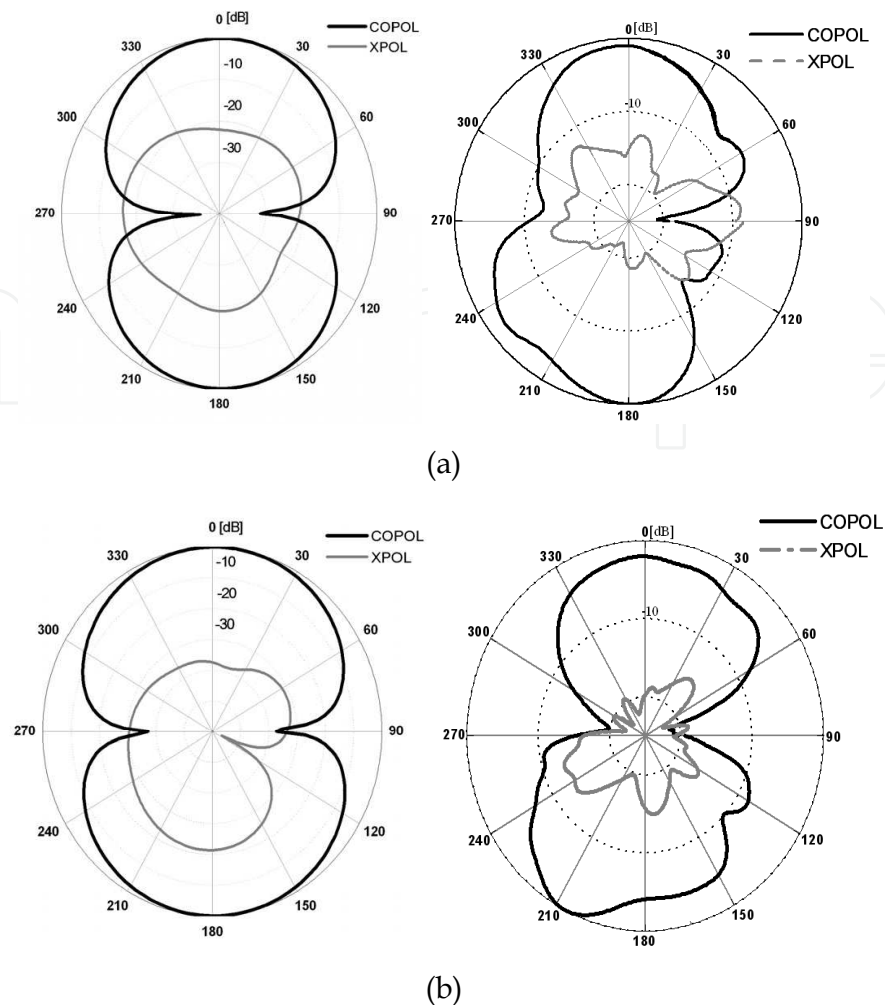
(a)

(b)

Fig. 25. E-plane radiation patterns of the miniaturized CLL-loaded printed dipole antenna of Section 1-3 at (a) 1.713GHz, and (b) 2.434GHz. (Right hand figures are measurements). From (Jafargholi et al., 2010), copyright © 2010 by Praise Worthy Prize, S. r. l.

3. Acknowledgment

4. References

[1] C. A. Balanis, *Advanced Engineering Electromagnetics*, John Wiley & Sons, New York, 1989.

[2] V. G. Veselago, "The electrodynamics of substances with simultaneously negative values of ε and μ," *Sov. Phys. Usp.*, vol. 10, no. 4, 509–514, 1968.

[3] M. Veysi, M. Kamyab, S. M. Mousavi, and A. Jafargholi "Wideband Miniaturized Polarization Dependent HIS Incorporating Metamaterials," *IEEE Antennas Wireless Propag. Letter*, vol. 9, 764-766, 2010.

[4] M. Rafaei Booket, M. Kamyab, A. Jafargholi and S. M. Mousavi, "Analytic Modeling and Implementation of The Printed Dipole Antenna loaded with CRLH Structures, " *Progressive In Electromagnetic Research B*, Vol. 20, 167-186, 2010.

[5] M. Veysi, M. Kamyab, J. Moghaddasi, and A. Jafargholi, "Transmission Phase Characterizations of Metamaterial Covers for Antenna Application," *Progressive In Electromagnetic Research Letter*, Vol.21, pp. 49-57, 2011.

[6] M. Rafaei Booket, A. Jafargholi, M. Kamyab, H. Eskandari, M. Veysi, and S. M. Mousavi, "A Compact Multi-Band Printed Dipole Antenna Loaded With Single-Cell MTM," Pending Publication in *IET Microwave Antenna Propag.*, 2011.

[7] A. Jafargholi, M. Kamyab, and M. Veysi, "PMC-based Waveguide-fed Slot Array," *ISRN Communications and Networking*, Hindawi, Vol. 2011, Article ID 941070, 5 Pages.

[8] A. Jafargholi, M. Kamyab, and M. Veysi, "Artificial Magnetic Conductor Loaded Monopole Antenna," *IEEE Antennas Wireless Propag. Letter*, vol. 9, 211-214, 2010.

[9] A. Jafargholi, M. Kamyab, M. Rafaei Booket, and M. Veysi, "A Compact Dual-band Printed Dipole Antenna Loaded with CLL-Based Metamaterials," *International Review of Electrical Engineering*, IREE, Vol. 5, No. 6, pp. 2710-2714, 2010.

[10] J. McVay, N. Engheta, and A. Hoorfar, "High-impedance metamaterial surfaces using Hilbert-curve inclusions," *IEEE Microwave Wireless Components Lett.*, vol. 14, no. 3, pp. 130–132, Mar. 2004.

[11] A. Erentok, P. Luljak, and R. W. Ziolkowski, "Antenna performance near a volumetric metamaterial realization of an artificial magnetic conductor," *IEEE Trans. Antennas Propagat.*, vol. 53, pp. 160–172, Jan. 2005.

[12] R. W. Ziolkowski and A. Kipple ,"Application of double negative metamaterials to increase the power radiated by electrically small antennas," *IEEE Trans. Antennas Propagat.*, vol. 51, no. 10, pp. 2626–2640, Oct. 2003.

[13] Q. Liu, P. S. Hall, and A. L. Borja ," Efficiency of Electrically Small Dipole Antennas Loaded With Left-Handed Transmission Lines," *IEEE Trans. Antennas Propagat.*, vol. 57, no. 10, pp. 3009–3017, Oct. 2009.

[14] S. D. Rogers, C. M. Butler, and A. Q. Martin, " Design and Realization of GA-Optimized Wire Monopole and Matching Network With 20:1 Bandwidth," *IEEE Trans. Antennas Propagat.*, vol. 51, no. 3, pp. 493–502, March. 2003.

[15] A. Erentok, and R. W. Ziolkowski, "Metamaterial-Inspired Efficient Electrically Small Antennas" *IEEE Trans. Antennas Propagat.*, vol. 56, pp. 691–707, March 2008.

[16] A. Erentok, *Metamaterial-Based Electrically Small Antennas*, Ph.D. dissertation at University of Arizona, 2007.

[17] J. Zhu, M. A. Antoniades, and G. V. Eleftheriades "A Compact Tri-Band Monopole Antenna With Single-Cell Metamaterial Loading" *IEEE Trans. Antennas Propagat.*, vol. 58, pp. 1031–1038, April. 2010.

[18] M. A. Antoniades and G. V. Eleftheriades, "A broadband dual-mode monopole antenna using NRI-TL metamaterial loading," *IEEE Antennas Wireless Propag. Lett.*, vol. 8, pp. 258–261, 2009.

[19] J. Zhu, M. A. Antoniades, and G. V. Eleftheriades, "A tri-band compact metamaterial-loaded monopole antenna for WiFi and WiMAX applications,"presented at the *IEEE Antennas and Propagation Society Int. Symp.*, Jun. 2009.

[20] J. Zhu and G. V. Eleftheriades, "Dual-band metamaterial-inspired small monopole antenna for WiFi applications," *Electron. Lett.*, vol. 45, no. 22, pp. 1104–1106, Oct. 2009.

[21] H. Iizuka, P. S. Hall, and A. L. Borja, "Dipole Antenna With Left-Handed Loading" *IEEE Antennas Wireless Propag. Lett.*, vol. 5, pp. 483–485, 2006.

[22] H. Iizuka, and P. S. Hall, "Left-Handed Dipole Antennas and Their Implementations" *IEEE Trans. Antennas Propagat.*, vol. 55, pp. 1246–1253, May 2007.

Metamaterial

Edited by Dr. Xun-Ya Jiang

In-depth analysis of the theory, properties and description of the most potential technological applications of metamaterials for the realization of novel devices such as subwavelength lenses, invisibility cloaks, dipole and reflector antennas, high frequency telecommunications, new designs of bandpass filters, absorbers and concentrators of EM waves etc. In order to create a new devices it is necessary to know the main electrodynamical characteristics of metamaterial structures on the basis of which the device is supposed to be created. The electromagnetic wave scattering surfaces built with metamaterials are primarily based on the ability of metamaterials to control the surrounded electromagnetic fields by varying their permeability and permittivity characteristics. The book covers some solutions for microwave wavelength scales as well as exploitation of nanoscale EM wavelength such as visible specter using recent advances of nanotechnology, for instance in the field of nanowires, nanopolymers, carbon nanotubes and graphene. Metamaterial is suitable for scholars from extremely large scientific domain and therefore given to engineers, scientists, graduates and other interested professionals from photonics to nanoscience and from material science to antenna engineering as a comprehensive reference on this artificial materials of tomorrow.

INTECH
open science | open minds